AS5500: Rotation Curves and Dark Matter Halos from MaNGA data

Rosie Braunholtz

Supervisor: Dr Anne-Marie Weijmans

Word count: 3963

1 Abstract

I present Hα rotation curves for a sample of 12 disk galaxies from the SDSS MaNGA survey. Rotation curves are obtained with DiskFit and are then fitted with potential models from the new python tool which implements galpy: GalRotpy. Bulge and DM fractions are found and compared with those from literature. There were no similarities nor any correlation between DM halo and stellar fraction found for these galaxies.

2 Introduction

Kinematic data from disk-like galaxies allow us to study the dynamical properties of the galaxy and it's stars and interstellar gas. It also provides us information on the structure, evolution and formation history of the galaxy. (Sofue and Rubin, 2001)

Rotation curves of spiral galaxies were first assumed to have a Keplerian decline, however observations proved that rotation curves remained flat in the outer regions (Bottema and Pestaña, 2015). This discrepancy in theory versus observations was explained by the existence of dark matter. The first detailed observations in HI of large disk galaxies showed a rotation which remained flat well beyond the luminous matter. Now it is believed that dark matter in galaxies resides in a halo which extends beyond the stars. This has been confirmed in numerous studies over the years. (Tiley et al., 2019)

Decomposing rotation curves into mass components is a useful method for studying spiral galaxies' dynamical structure, and it complements photometric decomposition of the luminous bulge and disc. Rotation curves can be used to determine the mass ratio of the bulge and/or disc to the dark halo. The bulge/disk to dark halo mass ratio is often taken as an indicator for cosmological structure, formation and evolution and is used as selection critieria when searching for particular types of galaxies. The de Vaucouleurs or Sersic law and exponential thin disk models are commonly used for the bulge and disk, respectively. For the dark halo the NFW (Navarro-Frenk- White) (Navarro et al., 1996) model and isothermal sphere model are the most commonly used (Sofue, 2013).

Emission lines from cold gas such as HI gas are commonly used to derive rotation curves because they have a small velocity dispersion and extend farther out the disk than the luminous matter. Long slit spectra can be used to evaluate the rotation curve from emission lines for optical measurements of Hα or stars. More complicated methods, such as Fabry-Perot spectographs or integral field units, provide more velocity detail, but they take longer and are therefore more costly. HI is perhaps the most preferred cold gas to obtain kinematics of spiral galaxies compared to other tracers because it extends much further out than the optical disk and in general is more uniformly distributed. (Sofue and Rubin, 2001) However measuring H emission is a lot less expensive than measuring the velocity of HI as it doesn't need a radio telescope. In addition Hα's emission line is much stronger than the absorption line from stars and it is much colder. Meaning the velocity dispersion will be smaller giving a more accurate circular velocity.

In this paper I describe the method of obtaining rotation curves and mass fractions from stellar kinematics and Hα gas for a sample of galaxies taken from the SDSS MaNGA survey (Bundy et al., 2015).

This paper is organized as follows: in Section 3 I describe the MaNGA survey and my sample, Section 4 I describe the methods for obtaining the rotation curve and DM fractions using DiskFit and GalRotpy. The results are presented in Section 5. My analysis and comparison is discussed in Section 6.

3 Data

3.1 Overview of MaNGA survey

SDSS MaNGA (Mapping Nearby Galaxies at APO) is a galaxy integral-field spectroscopic survey within the fourth generation Sloan Digital Sky Survey (SDSS-IV). Its aim is to provide insight into galaxy formation, evolution, merging, and death by mapping the structure and kinematics of 10,000 galaxies. The survey covers a broad field of view and maps the kinematics and structure of galaxies out to 1.5 Re, or half-light radius (Bundy et al., 2015).

3.2 Sample

Three galaxies which are not in the sample are included in the table and data. These are two "test" galaxies which were chosen for their clean velocity fields and strong Hα data (MaNGA plate-IFU's 9501-9102 and 8309-9102) and also 7815-12705 which was chosen to compare with a rotation curve and mass fraction from a different model (private communication, S. Campbell).

The galaxies presented in this work have been selected using MARVIN [1] (Cherinka et al., 2020). A sample was made with an inclination between 0.45 and 0.55, this is because the software DiskFit cannot compute well with highly inclined or nearly face on galaxies, a g-r ≤ 1 colour was used to select late-type spiral galaxies predominantly, and a HI snr > 15 was used to open up the possibility of a future comparisons or studies with HI data. These parameters were made limited to get a small sample. In addition all galaxies were viewed on the MARVIN web tool and inspected so that Hα was present and resided within the bulk of baryonic matter. Some galaxies didn't have Hα and so weren't included. In total 9 galaxies were found.

A table of SDSS properties of all 12 galaxies are shown in table 1. The distance was calculated using zdist which is a distance estimate and H0 = 67.4 $\pm$ 0.5 km s-1 Mpc-1 from Planck Collaboration et al. (2020), assuming the base-ΛCDM cosmology. From now on I will refer to a galaxy by it's MaNGA plate-IFU number.

Galactic inclination angles, axis ratios, and absolute magnitudes are taken from the NASA-Sloan Atlas (Blanton et al., 2011).

Table 1: SDSS parameters of galaxies

SDSS	Plate-IFU	Ellipticity	Inclination	Pos.Angle (deg)	Redshift	Distance(Mpc)	elpetroMass ($M_\odot$)
J084128.25+251404.0	9501-9102	0.251308	41.52283	235.018303	0.0291841	129189.06	1.53E+10
J211557.49+093237.9	7815-12705	0.544285	62.88905	325.02542	0.0293012	133469.76	1.95E+10
J094843.63+440453.1	8458-12705	0.44225	56.09968	233.498352	0.0159101	74039.085	2.77E+10
J085705.73+514850.6	8244-12703	0.526548	61.74136	233.02668	0.0172316	79404.271	2.05E+09
J154533.53+300850.7	9041-12702	0.524125	61.58365	345.88289	0.0316281	141769.07	1.62E+10
J130528.69+335057.9	8323-12701	0.541918	62.73659	181.3234863	0.0237655	105734.75	2.22E+09
J141508.07+453541.4	8329-12704	0.452514	56.80525	296.132454	0.0159429	73863.644	3.08E+09
J111330.70+231817.6	8449-12704	0.505119	60.33809	261.60933	0.0207039	91382.862	3.28E+09
J080352.89+263652.8	8149-6104	0.519753	61.29845	271.34917	0.0204161	91005.497	1.12E+09
J145649.42+413546.8	8980-3704	0.523017	61.51149	349.68317	0.0162132	74967.112	5.85E+08
J075212.79+302127.5	8936-12703	0.53312	62.16804	340.50592	0.0143646	70472.987	1.58E+09
J140747.65+532213.6	8309-9102	0.349954	49.45494	323.59637	0.0831966	371816.97	4.85E+10

4 Rotation Curve and Decomposition Method

4.1 DiskFit

All of the rotation curves presented in this paper were carried out using DiskFit, a publicly-available code that fits non-axisymmetric models to either images or velocity fields of disk galaxies (Sellwood and Spekkens, 2015).

DiskFit fits for the disk center, disk ellipticity, disk position angle and bar position angle. For kinematic data, the disk systemic velocity is estimated. Users are required to supply DiskFit with a velocity field for kinematic fits. The velocity fields were taken from the Hα line provided by the MaNGA survey (Figure 1.) along with an uncertainties in velocity. Each spaxel corresponds to 0.5 arcseconds. The distance from the center of the galaxies in kpc was calculated using the distance from Table 2. An input text file is also required,which supplies the code with parameter values and initial guesses for the disk parameters. This includes position angle, inclination, ellipticity, disk center and systemic velocity. An estimation for the disk center was made by eye for each galaxy. Note the systemic velocity of MaNGA galaxies is zero as they correct to the galaxy's rest frame. DiskFit can also provide beam smearing correction but this did not cover the scope of this project. Most of these parameters are are shown in Table 2.

DiskFit uses minimum χ^2 estimation of the differences between a projected model and the data . The following model was applied to all galaxies:

$$V_{model} = V_{sys} + sin(i)\,[V_t\,cos(\theta) - V_{m,t}\,cos(2\theta_b)\,cos(\theta) - V_{m,r}\,sin(2\theta_b)\,sin(\theta)], \quad (1)$$

[1] https://sas.sdss.org/marvin/

where V_{sys} is systemic velocity V_t is the circular velocity, $V_{m,t}$ and $V_{m,r}$ are the tangential and radial components of non-circular flows with harmonic order m= 1 or m= 2, θ and θ_b are the azimuthal angles relative to the major axis and the non-circular flow axis, respectively, and i is the disc inclination. If m= 1, the model describes a lopsided flow; if m= 2 the model is bisymmetric,and describes a barred or elliptical flow (Spekkens and Sellwood, 2007) (Kuzio de Naray et al., 2012a)

DiskFit assumes that the inner disk is flat and that non-circular motions come from a fixed principal axis i.e.the non-axisymmetric kinematic model is bar-like(Kuzio de Naray et al., 2012b).

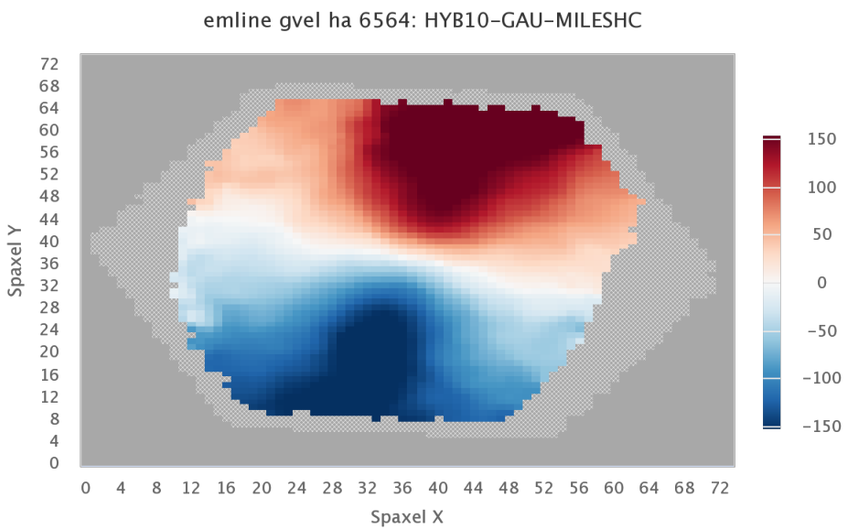

Figure 1: Hα velocity field for galaxy with plate-IFU 9041-12702 corrected to the galaxy's rest frame. Blue spaxels represent a blue-shifted Hα velocity and red spaxels represent a red-shifted Hα velocity (Bundy et al., 2015)(Cherinka et al., 2020)

4.2 Potential Theory

The stars, gas and dark matter in a galaxy all interact keeping with Newton's theory of gravity. The total mass of a disc-like galaxy is made up of various masses. The Poisson equation describes how the mass distribution equates to the gravitational potential:

$$\nabla^2\phi(x) = 4\pi G\rho(x), \tag{2}$$

with G the gravitational constant, ρ the mass density of the given system and $\phi(x)$ the gravitational potential. The mass distribution of a disc galaxy can be decomposed mainly into three mass components: bulge, disc, and dark matter halo.

The Miyamoto-Nagai potential expresses mass components of the bulge and the thin/thick disk of a galaxy and is a generalization of the Plummer and Kuzmin potentials. It is an axisymmetric potential defined in cylindrical coordinates (R,z) as:

$$\Phi_{MN}(R,z) = \frac{-GM}{\sqrt{R^2 + (a + \sqrt{z^2 + b^2})^2}}, \tag{3}$$

with a, b, M the length, height scales and mass enclosed at galactocentric distance R, respectively. The circular velocity is therefore (Binney and Tremaine, 2008):

$$V_c(R) = R\sqrt{\frac{GM}{(R" + (a+b)^2)^{\frac{3}{2}}}}. \tag{4}$$

The galactic disk is approximated by an exponential thin disk (Freeman, 1970) which can be considered as a flattened spheroid. The potential for an axisymmetric disc (when z$\rightarrow$ 0) is:

$$\Phi(R,0) = -4G\int_0^\infty \frac{da}{\sqrt{R^2 - a^2}}\frac{d}{da}\int_a^\infty \frac{R'\Sigma(R')dR'}{\sqrt{R'^2 - a^2}}, \tag{5}$$

with galactocentric radius R from the centre and axis a of the spheroid. Assuming the mass to light ratio is uniform, the surface density profile is:

$$\Sigma_d(R) = \Sigma_0\, exp(-R/h_r), \tag{6}$$

known as the exponential disc, where $\Sigma_0 = 2\rho qa$ and h_r are the central surface mass density and the radial scale respectively. For this model the total disc mass is given by :

$$M_d = 2\pi h_r^2 \Sigma_0. \tag{7}$$

One of the most commonly used dark matter halo profiles is the Navarro-Frenk-White (NFW) profile. Navarro et al. (1996) used simulations to study dark halos and found that galaxy and cluster halos were shown to have mass-density profiles approximated by the double power law:

$$\frac{\rho(r)}{\rho_{crit}} = \frac{\delta_c}{(r/r_s)(1 + r/r_s)^2}$$

where r_s is a scale radius, δ_c is a characteristic (dimensionless) density, and ρ_{crit} is the critical density. The NFW profile is called 'universal' since it operates for a wide range of halo masses, from individual galaxies to galaxy cluster halos.

The enclosed mass withing a radius r is

$$M_{NFW}(\leq r) = M_0 \left[ln(1 + \frac{r}{a}) - \frac{r/a}{1 + r/a} \right], \tag{8}$$

where $M_0 = 4\pi\rho_0 a^3$, this leads to potential

$$\Phi_{NFW}(r) = -4\pi G\rho_0 a^2\, \frac{ln(1 + r/a)}{r/a}, \tag{9}$$

and so the circular velocity is

$$V_c(R) = \sqrt{\frac{G}{R} M_{NFW}(\leq R)}. \tag{10}$$

(Binney and Tremaine, 2008)(Granados et al., 2017)

4.3 GalRotpy

GalRotpy is a Python3-based method that uses the rotation curve of disc-like galaxies to calculate the contribution of each mass variable to the gravitational potential. GalRotpy performs a parametric fit of a given rotation curve, which relies on a MCMC procedure which implements the package galpy.

GalrotPy divides a disk like galaxy into their main components: spheroidal bulge, thin and thick discs, spheroidal stellar and Dark Matter halos. The gravitational potential for each component are; a Miyamoto-Nagai potential model for the bulge/core and the thin/thick disc, an exponential disc, and a NFW potential or the Burkert potential for the Dark Matter halo (Granados et al., 2017)(Bovy, 2015) [2].

It is required to give GalRotpy an initial value for the mass in $M_\odot$ for the Miyamoto-Nagai and dark halo potentials. For the exponential disk an initial mass density $M_\odot/pc^2$ is needed. A crude estimate of the composition was made using the mean values for bulge, disk and halo decompositions from Table 2 in paper Sofue (2016). The fractions for each component were calculated and then multiplied by the stellar mass for petrosian flux given by NASA-Sloan Atlas. The initial density was calculated with the stellar mass and the area of a circle from the galaxy's radius. The galactocentric distance and height scales in kpc for each component also needed to be provided and these were again taken from Table 2 in Sofue (2016), the same distance and height scales were used for each galaxy. The input mass component values for each galaxy can be found in Table 2.

To find a better estimation of the parameters galpy (Bovy, 2015) uses the package `emcee` to implement a Markov chain Monte Carlo (MCMC) algorithm, where it obtains the posterior probability distribution $P(\theta, D, M)$ with θ, D and M being the parameters involved, the data used and the model respectively. For further information please read the documentation.

[2] https://github.com/andresGranadosC/GalRotpy

Table 2: Input mass decompositions for GalRotpy

SDSS	Plate-IFU	Elpetro($M_\odot$)	Bulge($M_\odot$)	Disk($M_\odot$)	Halo($M_\odot$)
J084128.25+251404.0	9501-9102	1.53E+10	4.59E+09	1.07E+10	2.6E+11
J211557.49+093237.9	7815-12705	1.95E+10	5.85E+09	1.37E+10	3.32E+11
J094843.63+440453.1	8458-12705	2.77E+10	8.3E+09	1.94E+10	4.7E+11
J085705.73+514850.6	8244-12703	2.05E+09	6.14E+08	1.43E+09	3.48E+10
J154533.53+300850.7	9041-12702	1.62E+10	4.86E+09	1.13E+10	2.75E+11
J130528.69+335057.9	8323-12701	2.22E+09	6.65E+08	1.55E+09	3.77E+10
J141508.07+453541.4	8329-12704	3.08E+09	9.23E+08	2.15E+09	5.23E+10
J111330.70+231817.6	8449-12704	3.28E+09	9.83E+08	2.29E+09	5.57E+10
J080352.89+263652.8	8149-6104	1.12E+09	3.37E+08	7.87E+08	1.91E+10
J145649.42+413546.8	8980-3704	5.85E+08	1.75E+08	4.09E+08	9.94E+09
J075212.79+302127.5	8936-12703	1.58E+09	4.73E+08	1.1E+09	2.68E+10
J140747.65+532213.6	8309-9102	4.85E+10	1.46E+10	3.4E+10	8.25E+11

5 Results and analysis

Using the input parameters from Table 1 each galaxy was run through DiskFit. I used an m=2 second harmonic. DiskFit fit for non-axisymmetric flow meaning it is able to fit for irregularities and galaxies which have bars. I used DiskFit to fit for the galaxy centre, inclination, systemic velocity, and position angle of the major axis. The minimum ring spacing was kept the same for all galaxies, the spatial resolution of the data was 2.5" however I did not correct for beam smearing.

The rotation curve for each galaxy was then run through GalRotpy through a file containing the distance from the centre in kpc and km/s for the velocity and its uncertainty. GalRotpy fit for models of the bulge, bulge-exponential disk, bulge-exponential disk-halo, exponential disk and exponential disk-halo. The NFW profile was used to model the dark halo. Following the advice of the documentation, the fitting process is linked to how well the walkers behave. For each galaxy 20 walkers and 200 steps were used and it was ran 10 times. It is worth noting that not every combination of contributions GalRotpy will provide reliable results, some will diverge or converge to unphysical values. Also the initial guess parameters needed to reproduce the data as well as possible, other wise the results are more likely to diverge. This should be kept in mind when moving onto the results.

The rotation curves for each galaxy with mass decompositions are found in figures 2 to 13. Many of the rotation curves have kinks and bumps. The final parameters of the mass compositions of the galaxies with the 95th uncertainty percentiles can be found in tables 3 to 7.

5.1 Rotation Curves and DM fractions

The rotation curves for all galaxies were fit with the GalRotPy model fits for the bulge, bulge + disk, bulge + disk + halo, disk and disk +halo. The masses and mass fractions for each galaxy can also be found in tables 3, 4, 5, 6 and 7. It is clear at a first glance that results are uneven depending on the galaxy meaning my results have no clear pattern. In this section I will describe the fit of the model on each individual galaxy. For most galaxies a NFW halo is not needed as I would expect since I am only taking data from within 1.5 half-light radius of the galaxy, whereas dark matter resides more in the outskirts of a galaxy.

Figure 2: 9501-9102

The errors for each data point are quite low. For this galaxy the best fits are when a bulge is present, again not surprising since I am only looking within 8kpc. The model fits the data slightly better without the presence of the dark matter halo.

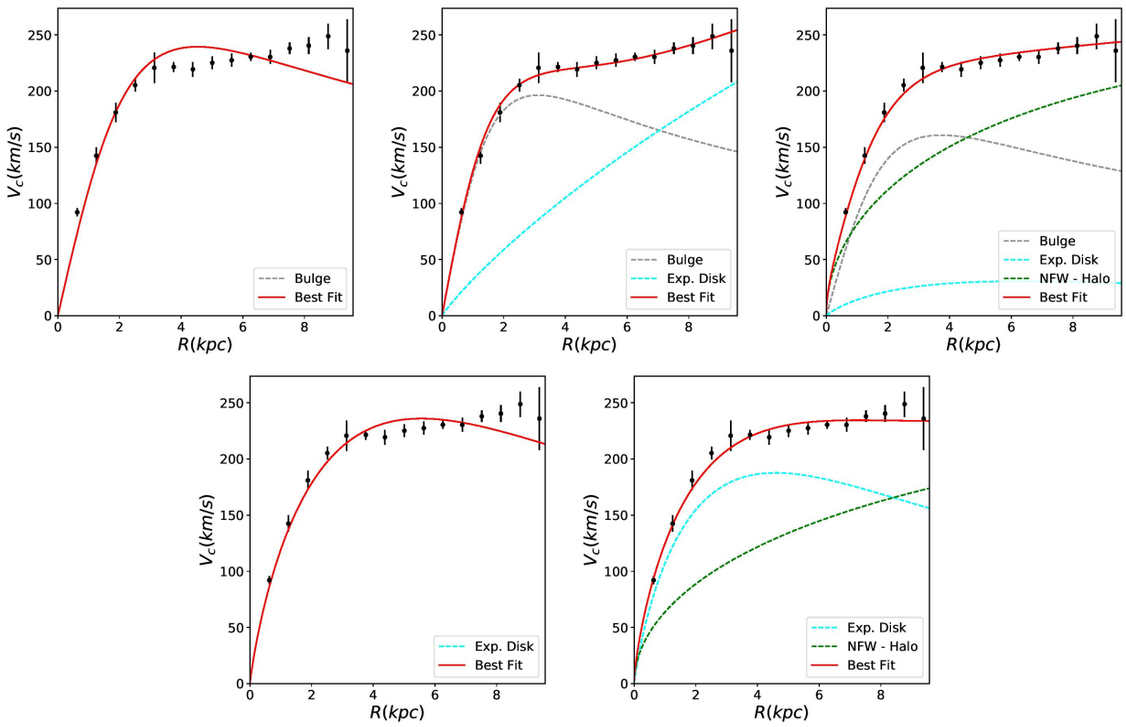

Figure 3: 7815-12705

7815-12705 was again not part of the sample but was chosen to compare with a rotation curve and mass fraction from mass modelling. The rotation curve and kinematic model fits can be seen in Figure. 3. The error bars show a large error in velocity which will affect the accuracy of the fit and mass fractions. The bulge-disk model and bulge-disk-halo model fit the data similarly meaning that a dark halo is not needed to fit the data.

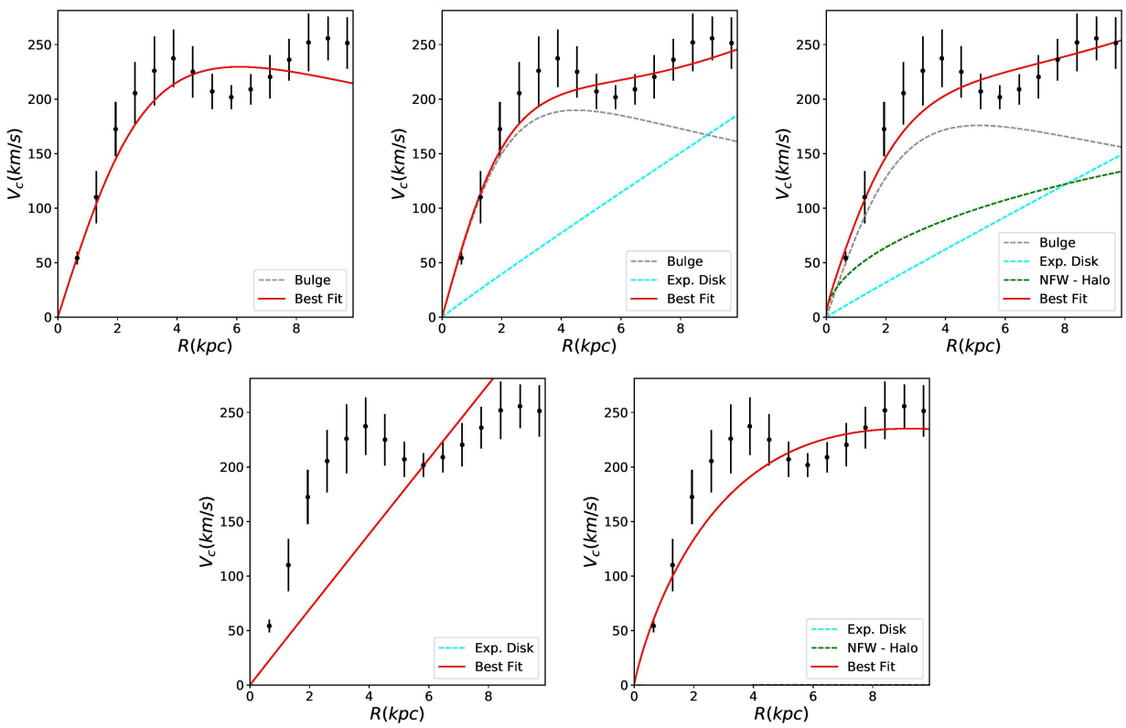

Figure 4: 8458-12705
There is not a large disparity between the fits with a dark halo and those without. The model fits the data best without a bulge and only with the exponential disk.

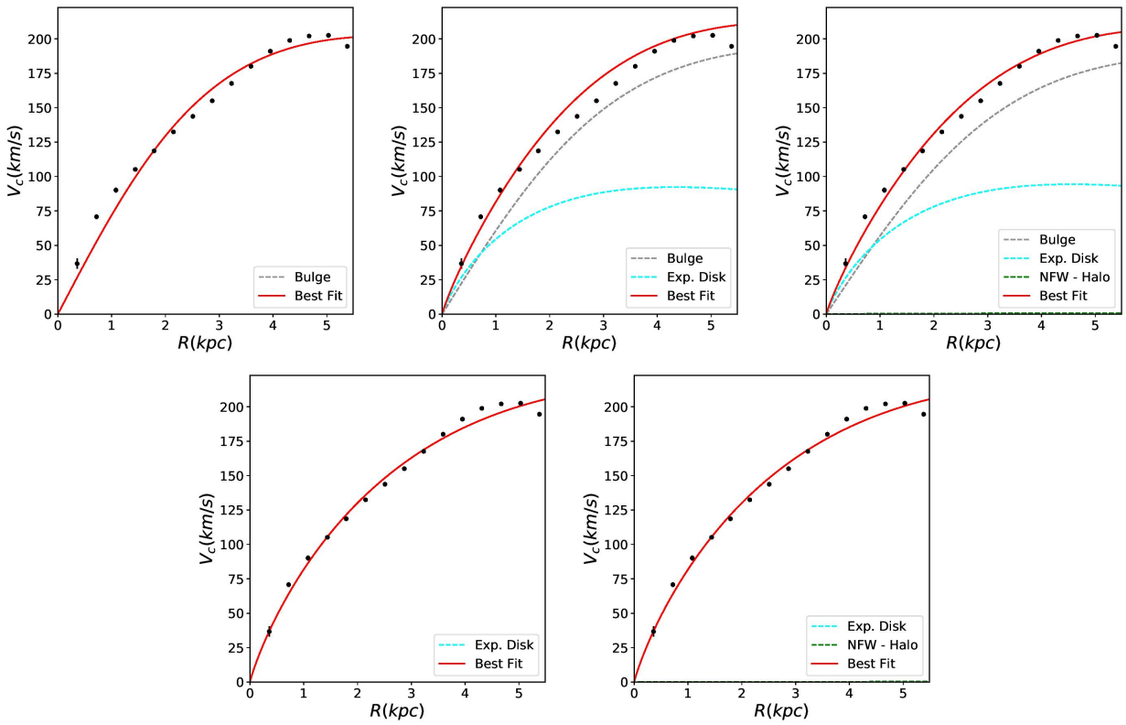

Figure 5: 8244-12703
For this galaxy the bulge-disk composition fits the data points best, and adding a dark halo fits it slightly worse

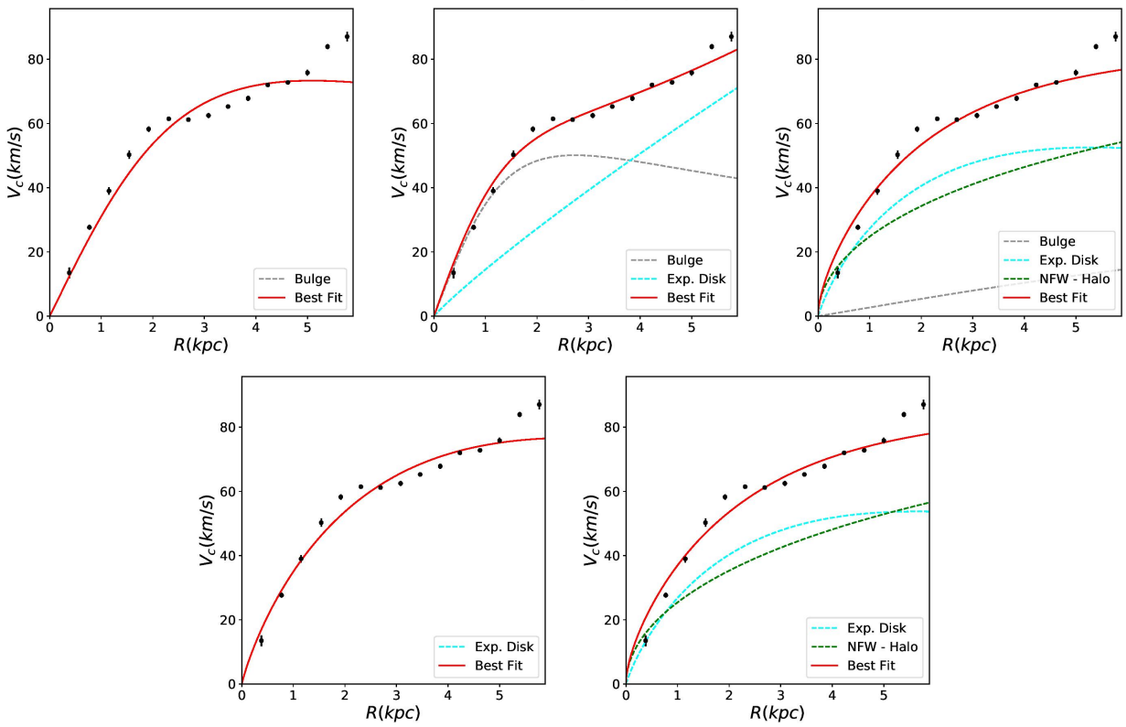

Figure 6: 9041-12702

Looking at the fit on the graph they all fit very similar. Refering to the tables it can be seen that the χ^2 value is the lowest with just an exponential disk, and least well fit when using a bulge-disk composition.

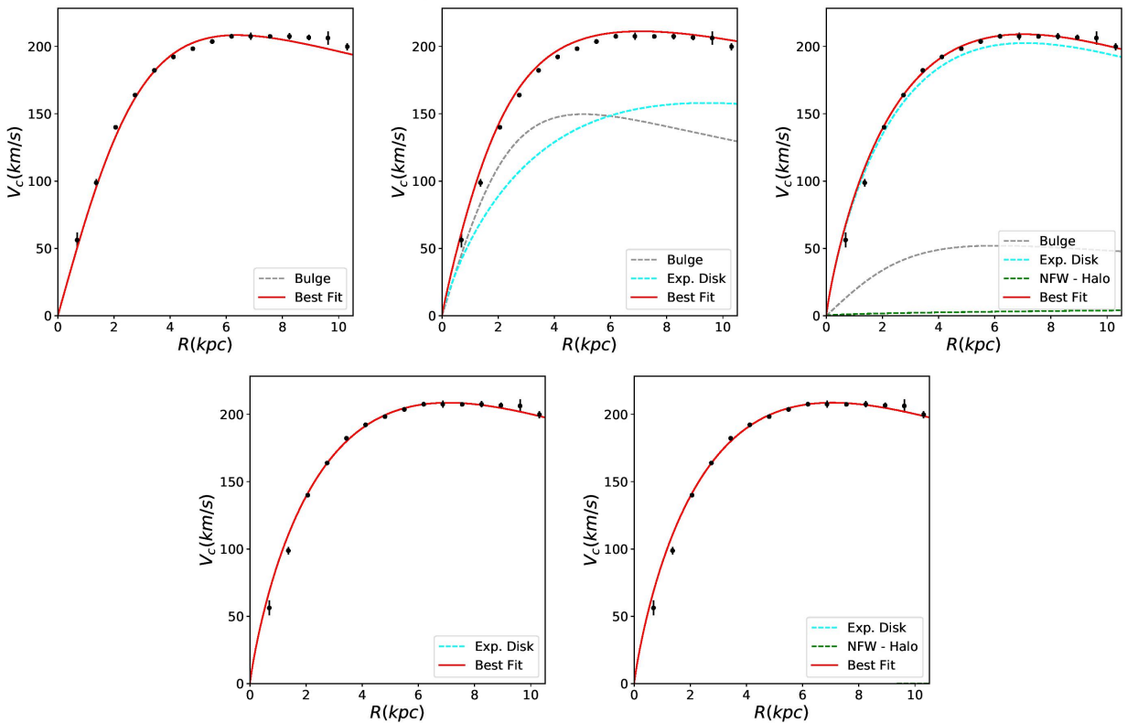

Figure 7: 8323-12701

This galaxy has small differences in the fit. Table 6 shows that the lowest χ^2 value is for an exponential disk model.

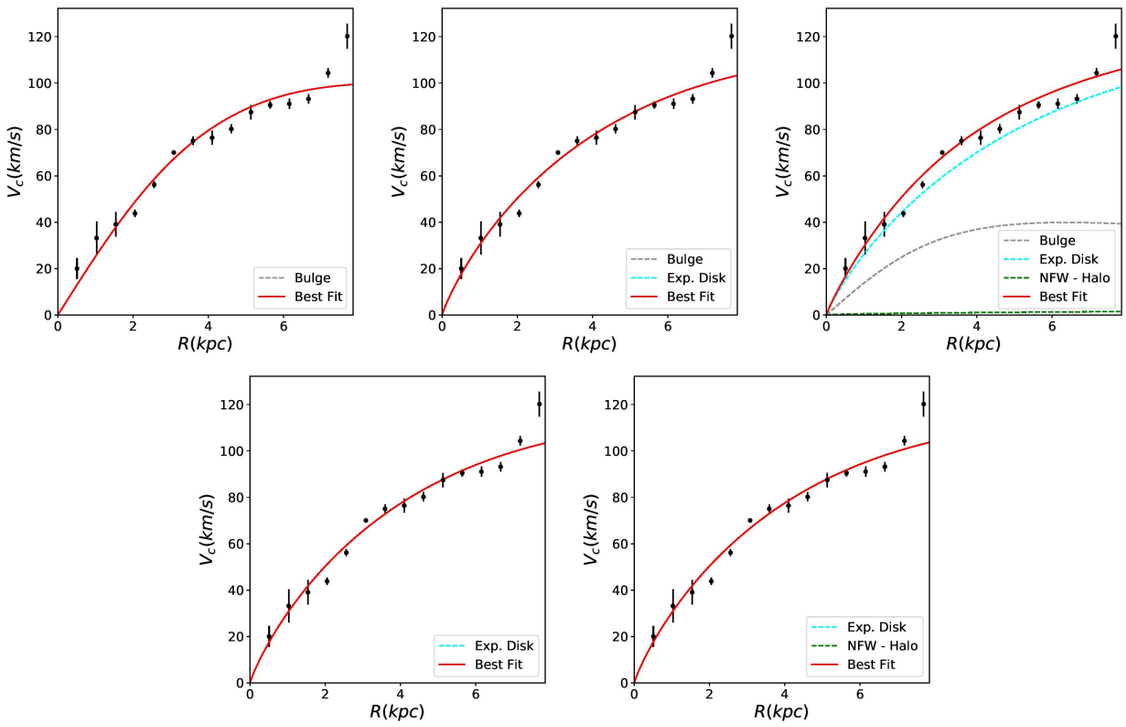

Figure 8: 8329-12704
This galaxy has small differences in the fit. Looking at χ^2 in Table 7. the disk-halo model is the best fit. Meaning that a halo is prominent in the inner regions of the galaxy. The halo mass fraction is 0.89.

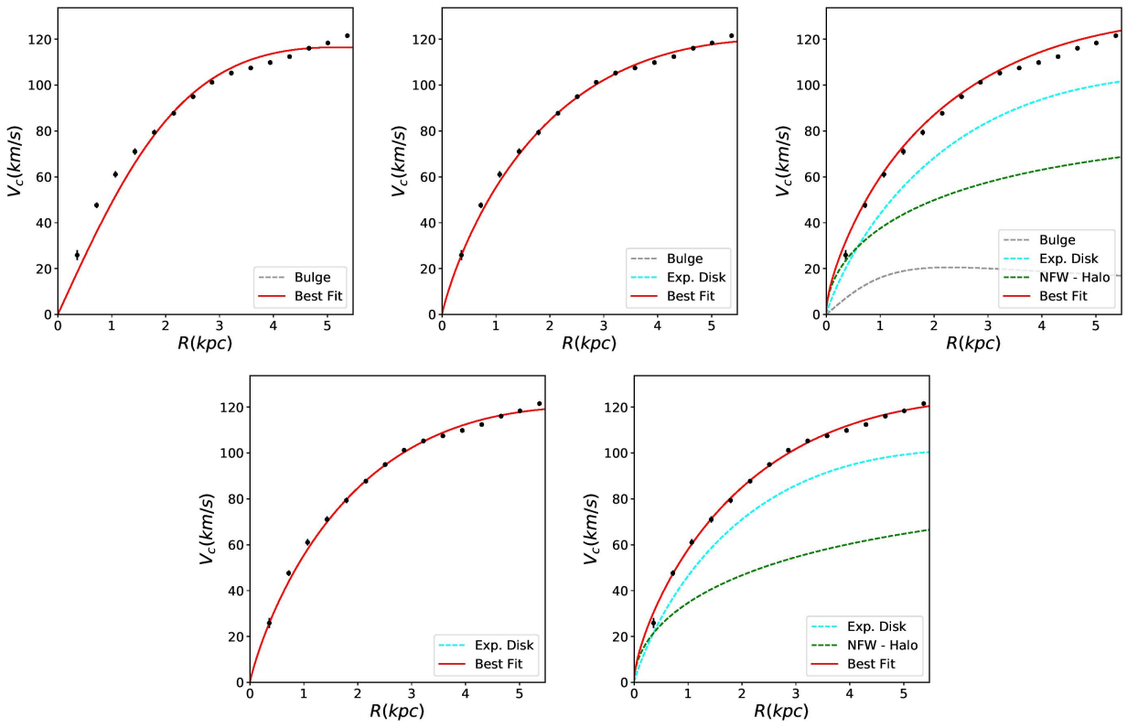

Figure 9: 8449-12704
From Table 1. the best fitting model is using only the bulge component, suggesting that this galaxy has a significant bulge despite it being a spiral.

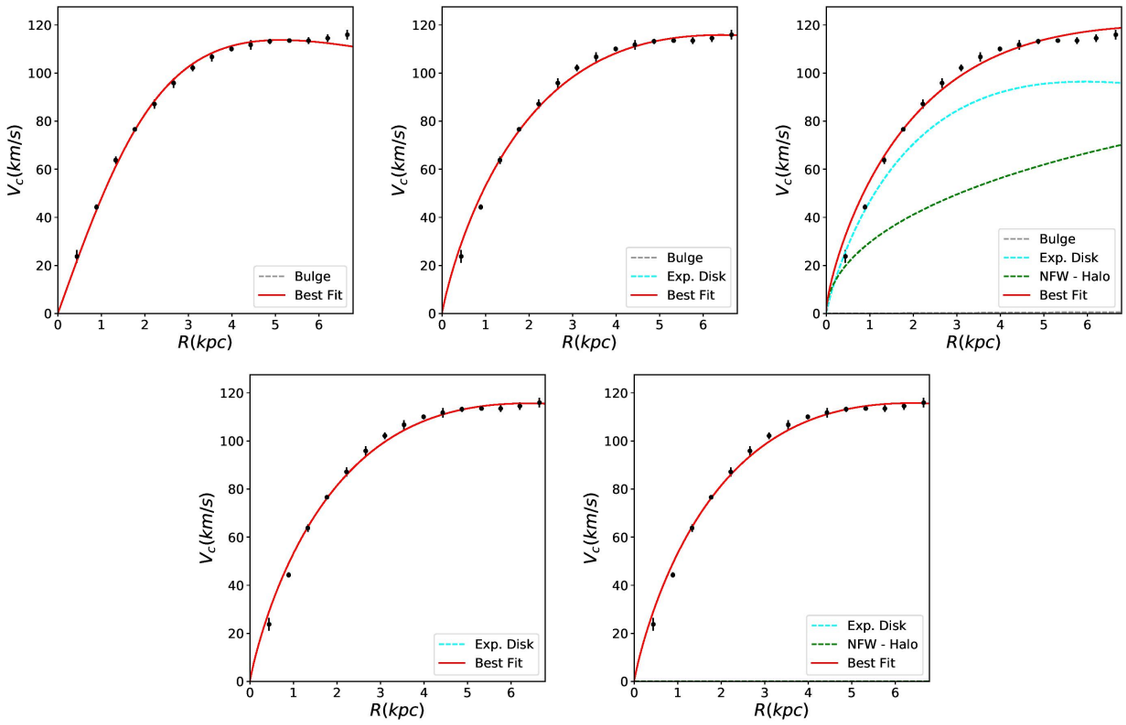

Figure 10: 8149-6104
8149-6104 has significant errors in the velocity which has severely impacted the quality of the fit. It appears a model including a dark halo fit's the data points slightly better however there is no certainty on this.

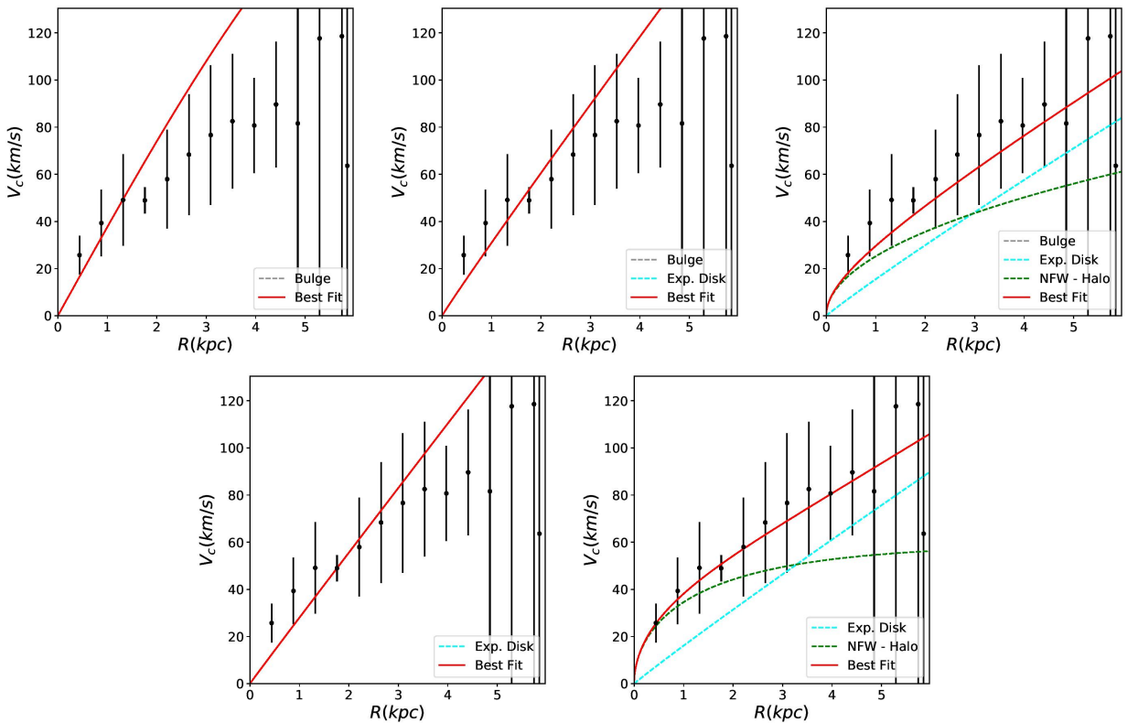

Figure 11: 8980-3704
This galaxy is similar in that the errors are too large to be able to say if a model fits the data points better than another one. This may be due to the size of the area covered being only 4kpc.

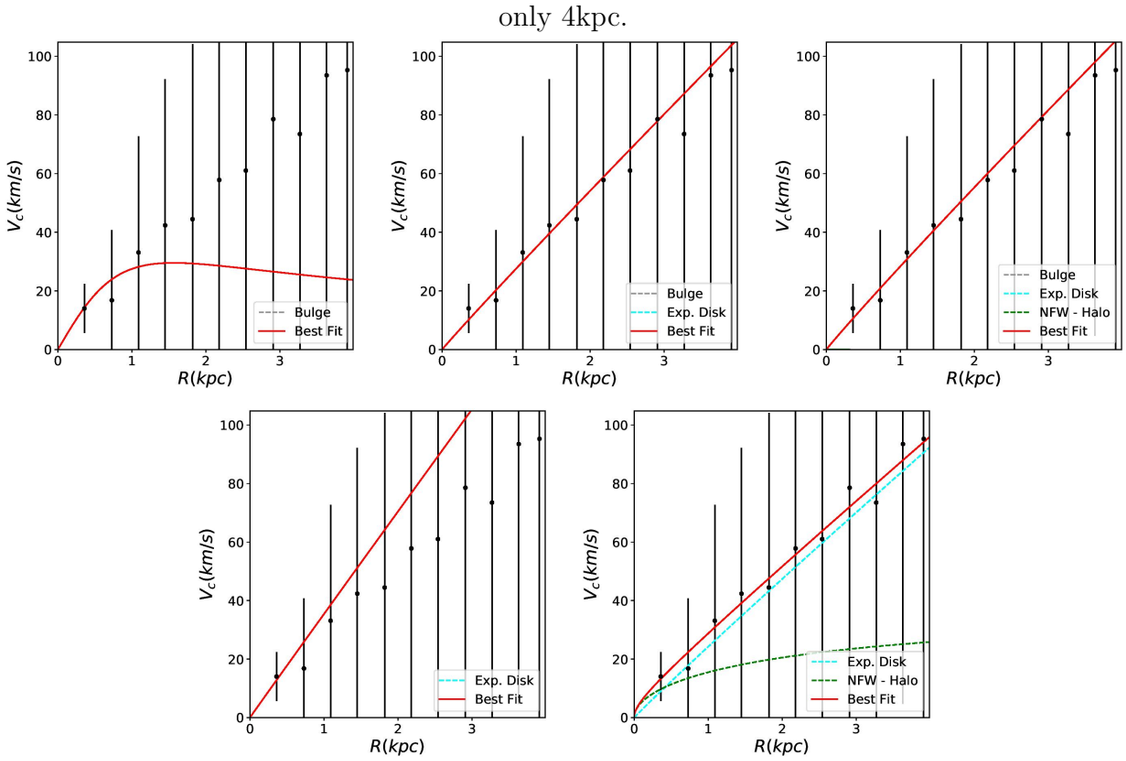

Figure 12: 8936-12703

There is a slight kink in the rotation curve, perhaps due to something not visible in the galaxy. The best fitting model is one using bulge and disk components which can be seen from table 4.

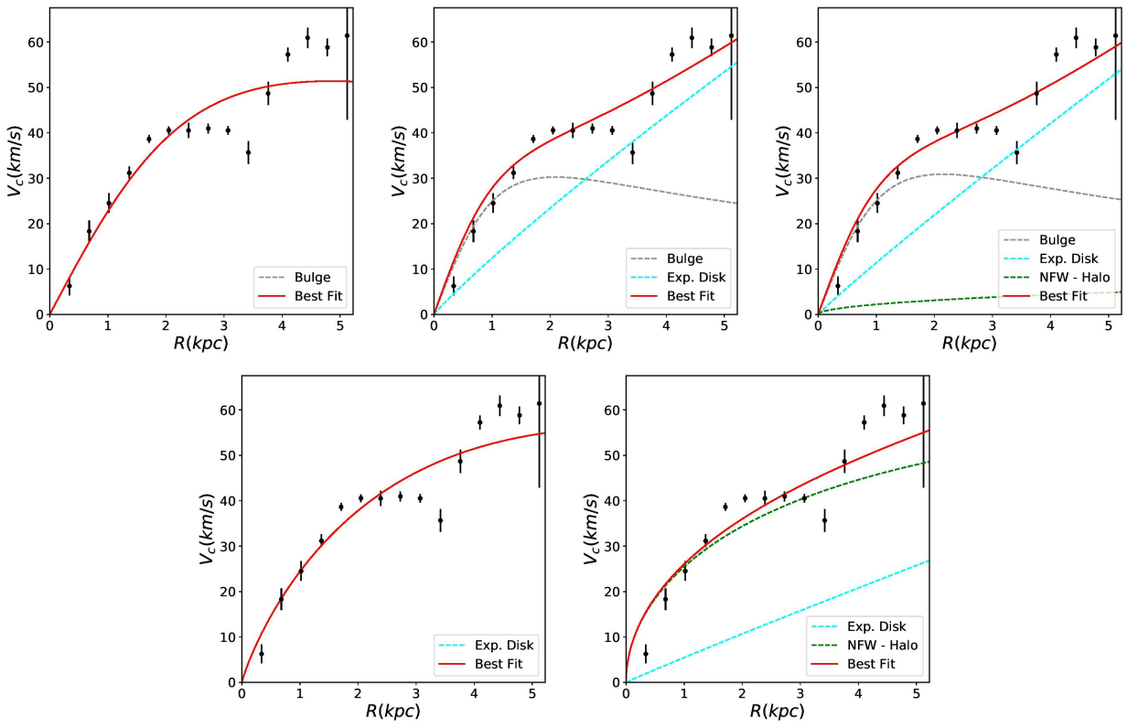

Figure 13: 8309-9102

8309-9102 seems to be a bulge dominated in the centre as this is the model which fits best.

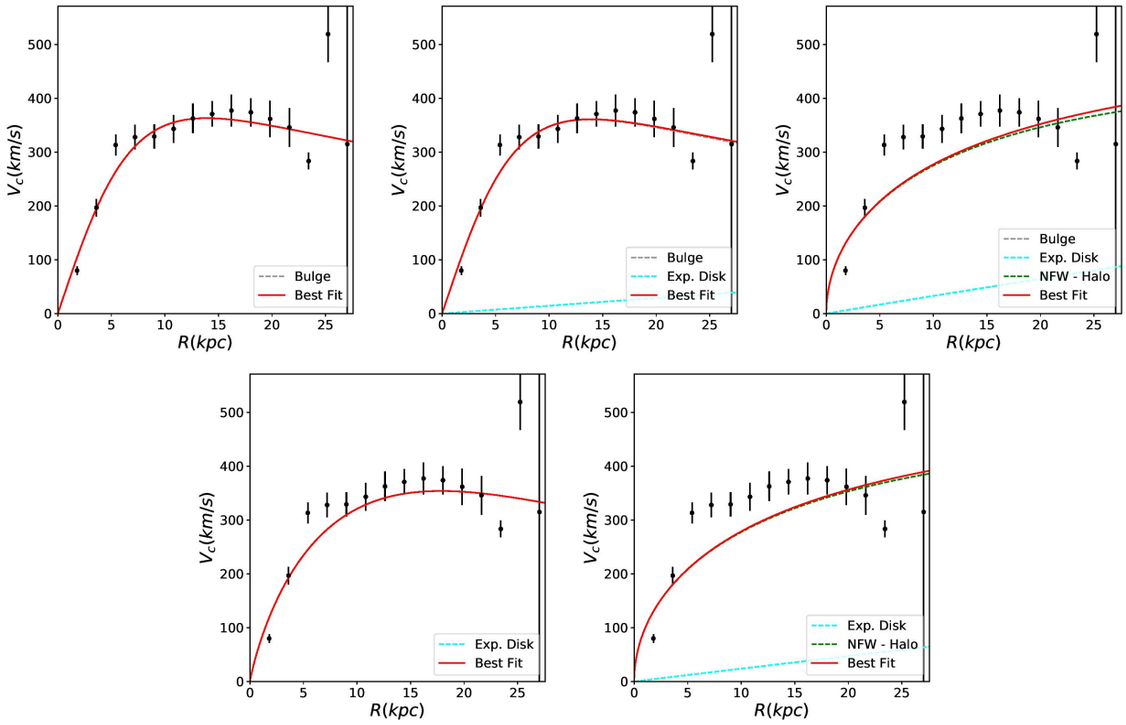

Table 3: Mass and $\chi^2$of sample obtained using GalRotpy for a model using only the bulge component with 95th percentile error.

Galaxy	Bulge($M_\odot$)	-95(%)	+95(%)	χ^2
9501-9102	1.11E+11	5.35	6.13	7.30
7815-12705	1.37E+11	18.59	27.38	1.82
8458-12705	1.08E+11	1.86	2.26	48.10
8244-12703	1.17E+10	3.75	3.73	51.04
9041-12702	1.18E+11	1.79	1.93	6.93
8323-12701	3.77E+10	9.88	10.66	6.10
8329-12704	3E+10	2.61	2.90	27.37
8449-12704	2.83E+10	3.10	2.95	1.54
8149-6104	4.93E+11	97.29	21086.25	2.97
8980-3704	5.85E+08	9.32	12.33	0.30
8936-12703	5.48E+09	15.73	17.78	14.99
8309-9102	7.83E+11	13.72	14.36	3.59

Table 4: Mass and χ^2 of sample obtained using GalRotpy for a model using only the bulge and disk components with 95th percentile errors.

Galaxy	Bulge($M_\odot$)	b-95(%)	b+95(%)	Disk($M_\odot$)	d-95(%)	d+95(%)	B/T	B/T -(%)	B/T+(%)	χ^2
9501-9102	5.14E+10	24.04	23.90	1.01E+13	97.41	3.23E+04	0.01	24.04	23.90	0.52
7815-12705	6.92E+10	34.44	64.87	2.26E+27	100.00	1.19E+09	0.00	34.44	64.87	1.11
8458-12705	1.13E+11	26.82	12.08	1.01E+10	96.22	154.63	0.92	26.82	12.08	140.98
8244-12703	2.94E+09	7.99	12.00	1.85E+14	98.20	1.19E+04	1.59E-05	7.99	12.00	16.17
9041-12702	4.82E+10	31.16	34.83	6.5E+10	22.51	19.47	0.43	31.16	34.83	21.70
8323-12701	2.74E+11	98.56	1.71E+07	4.63E+10	20.04	38.28	0.86	98.56	1.71E+07	7.44
8329-12704	4.01E+12	98.74	3.31E+05	2.54E+10	4.84	5.81	0.99	98.74	3.31E+05	6.35
8449-12704	2.02E+12	92.89	3.97E+06	2.41E+10	5.96	130.49	0.99	92.89	3.97E+06	4.17
8149-6104	2.44E+14	99.99	3.64E+16	1.45E+28	100.00	7.90E+47	1.68E-14	99.99	3.64E+16	1.42
8980-3704	1.87E+15	100.00	2.84E+17	7.02E+30	100.00	1.75E+48	2.67E-16	100.00	2.84E+17	0.05
8936-12703	8.15E+08	25.42	35.16	5.35E+14	98.68	3.15E+06	1.53E-06	25.42	35.16	9.38
8309-9102	7.68E+11	14.03	17.59	6.13E+30	100.00	1.08E+08	1.25E-19	14.03	17.59	4.31

Table 5: Mass and χ^2 of sample obtained using GalRotpy for a model using bulge, disk and dark halo components with 95th percentile errors.

Galaxy	Bulge ($M_\odot$)	b-95(%)	b+95(%)	Disk($M_\odot$)	d-95(%)	d+95(%)	Halo($M_\odot$)	h-95(%)	h+95(%)
9501-9102	4.12E+10	30.83	41.98	1.82E+09	99.94	9.43E+05	3.29E+12	63.08	238.19
7815-12705	6.77E+10	55.82	67.07	4.47E+26	99.10	1.37E+11	1.32E+12	100.00	802.90
8458-12705	1.10E+11	54.30	19.65	1.11E+10	89.99	421.81	5.90E+03	99.99	7.58E+04
8244-12703	6.13E+09	79.77	434.85	3.98E+09	61.02	68.21	2.53E+11	53.38	102.28
9041-12702	7.03E+09	94.63	229.02	8.13E+10	13.55	4.95	1.30E+07	100.00	6.18E+05
8323-12701	4.34E+09	93.09	437.14	6.00E+10	42.58	1.56E+03	3.13E+04	100.00	2.05E+07
8329-12704	4.14E+08	93.81	327.72	2.17E+10	23.28	45.40	1.07E+11	97.43	125.42
8449-12704	4.64E+07	96.79	1.57E+04	1.44E+10	55.79	61.18	8.53E+11	94.48	82.88
8149-6104	1.87E+11	97.18	4.28E+11	2.87E+19	98.93	1.21E+32	8.60E+12	100.00	546.11
8980-3704	9.84E+12	97.73	3.37E+18	5.83E+24	99.94	6.29E+52	4.93E-02	4.39E+04	4.98E+10
8936-12703	8.77E+08	27.68	43.80	5.78E+18	98.63	3.94E+06	2.90E+08	100.00	3.54E+03
8309-9102	5.08E+11	98.31	1.70E+07	3.20E+29	100.00	8.93E+17	1.60E+13	51.58	629.21

B/S	H/T	B/S -95(%)	B/S +95(%)	H/T -95(%)	H/T+95(%)	χ^2
0.96	0.99	42.90	3.99E+04	88.64	614.74	1.03
1.51E-16	2.96E-15	113.74	1.37E+11	140.79	1.37E+11	1.96
0.91	4.86E-08	73.83	46.72	111.81	7.58E+04	69.11
0.61	0.96	96.34	509.27	74.09	142.26	51.18
0.08	1.47E-04	95.75	229.79	101.05	6.18E+05	4.03
0.07	4.86E-07	101.40	1.52E+03	107.78	2.05E+07	10.32
0.02	0.83	96.57	330.79	126.62	163.10	24.74
3.22E-03	0.98	111.63	1.57E+04	132.51	116.25	11.69
6.53E-09	3.00E-07	138.67	1.21E+32	140.66	1.21E+32	0.64
1.69E-12	8.46E-27	139.78	6.29E+52	43901.07	6.29E+52	0.07
1.52E-10	5.02E-11	102.44	3.94E+06	140.46	3.94E+06	11.66
1.59E-18	5.00E-17	140.23	8.93E+17	112.52	8.93E+17	18.52

Table 6: Mass and χ^2 of sample obtained using GalRotpy for a model using only a disk component with 95th percentile error.

Galaxy	Disk($M_\odot$)	-95(%)	+95 (%)	χ^2
9501-9102	8.66E+10	6.75	8.42	2.46
7815-12705	1.91E+110	100.00	3.39E+49	10.66
8458-12705	1.13E+11	3.55	4.37	47.15
8244-12703	1.06E+10	5.54	6.42	31.13
9041-12702	8.58E+10	2.13	2.15	2.72
8323-12701	4.67E+10	17.66	24.96	5.73
8329-12704	2.55E+10	4.25	4.23	4.89
8449-12704	2.39E+10	4.39	5.34	3.19
8149-6104	2.01E+69	100.00	1.80E+41	0.81
8980-3704	4.55E+98	100.00	9.77E+64	0.13
8936-12703	6.21E+09	23.72	33.94	11.10
8309-9102	6.25E+11	16.63	20.79	5.63

Table 7: Mass and χ^2 of sample obtained using GalRotpy for a model using disk and dark halo components with 95th percentile errors.

Galaxy	Disk($M_\odot$)	d-95(%)	d+95(%)	Halo($M_\odot$)	h-95(%)	h+95(%)	H/T	H/T -95(%)	H/T +95(%)	χ^2
9501-9102	4.25E+10	40.68	68.64	4.82E+12	80.24	461.10	0.99	112.98	649.25	1.06
7815-12705	1.43E+11	30.02	69.78	4.20E+01	198.78	3.44E+05	2.94E-10	201.03	3.44E+05	1.87
8458-12705	1.13E+11	4.37	4.98	1.31E+05	103.93	3.43E+06	1.15E-06	104.03	3.43E+06	55.73
8244-12703	4.62E+09	67.78	43.74	3.64E+11	67.70	446.92	0.99	95.14	628.09	33.90
9041-12702	8.58E+10	2.63	2.53	6.96E-01	102.97	9.36E+09	8.11E-12	103.00	9.36E+09	3.22
8323-12701	4.72E+10	21.42	30.32	7.61E-03	2.65E+03	2.83E+06	1.61E-13	2653.36	2.83E+06	6.78
8329-12704	1.85E+10	27.96	17.05	1.48E+11	62.71	196.84	0.89	83.94	263.32	3.69
8449-12704	2.39E+10	5.35	5.02	5.10E+00	100.58	2.44E+07	2.13E-10	100.72	2.44E+07	3.77
8149-6104	1.54E+24	77.30	93.31	3.69E+10	53.33	115.67	2.40E-14	93.91	148.61	0.07
8980-3704	2.05E+27	67.58	176.72	1.17E+10	97.11	197.39	5.73E-18	118.31	264.94	0.01
8936-12703	9.15E+23	99.89	9.64E+07	7.59E+10	64.94	510.72	8.30E-14	119.15	9.64E+07	14.50
8309-9102	3.32E+39	100.00	5.99E+12	1.96E+13	52.38	344.27	5.91E-27	112.89	5.99E+12	13.43

6 Discussion and Conclusion

I expect the bulge/stellar mass fraction to be small for the sample because they are disk galaxies. Furthermore disk galaxies are expected to have (on average) a dominant dark matter fraction (Sofue, 2016). Comparing the bulge mass fraction to the dark halo fraction I would expect that disk galaxies with small bulges have a larger DM fraction, and those with larger bulges to have a smaller DM fraction. This was plotted on figure 14. What I would hypothesize to see according to literature is that as bulge size increases, the halo fraction would decrease giving a negative incline. With this sample there is no negative correlation with the data as I would expect. However this sample is very small and a larger number of galaxies would be needed to see if there was any relationship.

Simard et al. (2011) carried out photometric bulge+disk decomposition's for 1.12 million galaxies from SDSS Data. They used three different fitting models but in this comparison I use results taken from a free Sersic index n_b bulge + disk model. For more information please see their paper. Table 8 shows their results for my sample of galaxies. The disc and bulge light distribution are measured by the photometry of the galaxy.

Figure 15. shows Simard et al. (2011) results for the bulge fraction in the g-band compared to my results from table 4 using only the GalRotpy fit for bulge and disk components. For this comparison I assume the mass to light ratio is the same throughout the galaxy.

Galaxy 7815-12705 can be compared with a rough estimate of the dark matter fraction using Jeans Anisotropic MGE modeling method or JAM done by S. Campbell. This data was obtained using the HI follow up survey of MaNGA galaxies. The survey used single dish data and a double horned profile method was used to extract the rotation curves (Masters et al., 2019) . They used a NFW profile to model the dark matter in the galaxy. The HI rotation curve extends much farther out than the Hα data, but looking at the curve up to 10kpc the rotation curve and luminous and dark matter compositions look quite similar if I compare to figure 3. The dark matter fraction came out to be around 0.3. (private communication, S. Campbell). I can compare this to results from table 7 and 5 in which

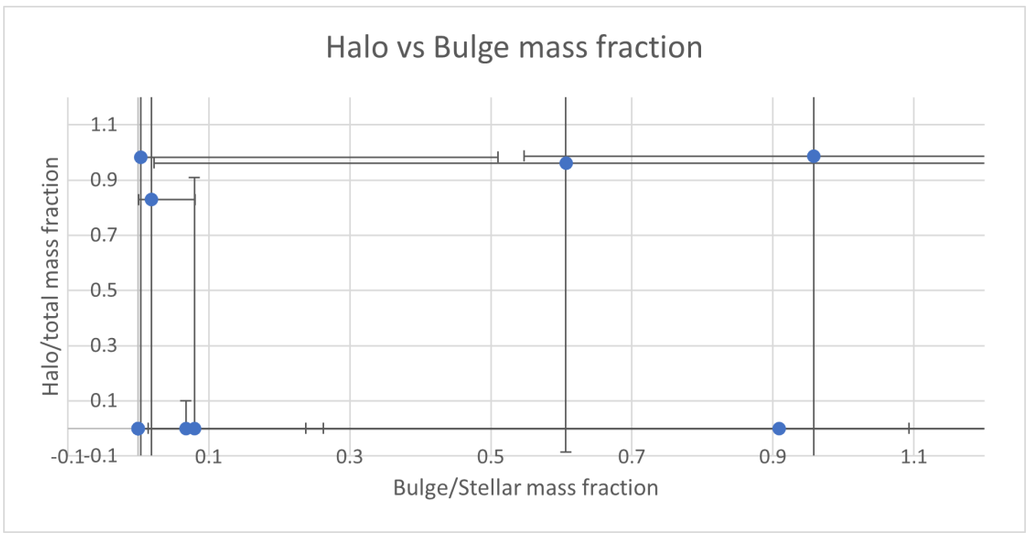

Figure 14: Bulge mass fraction vs DM fraction for all galaxies.

Table 8: Simard et al. (2011) bulge fractions for my sample of galaxies in the g and r band with errors.

Galaxy	z	(B/T)g	e_	(B/T)r	e_
J084128.25+251404.0	0.0293	0.02	0	0.04	0
J211557.49+093237.9	0.0293	0.09	0	0.17	0
J094843.63+440453.1	0.1589	0.85	0.03	0.97	0.03
J085705.73+514850.6	0.0173				
J154533.53+300850.7	0.0317	0.12	0	0.21	0
J130528.69+335057.9	0.0238	0.15	0.01	0.17	0.01
J141508.07+453541.4	0.016	0.58	0	0.66	0.01
J111330.70+231817.6	0.0208	0.05	0.02	0.03	0.02
J080352.89+263652.8	0.0204	0.36	0.01	0.42	0.02
J145649.42+413546.8	0.0162	0.2	0.01	0.24	0.01
J075212.79+302127.5	0.0146	0.9	0	0.88	0.01
J140747.65+532213.6	0.0832	0.24	0.01	0.33	0.01

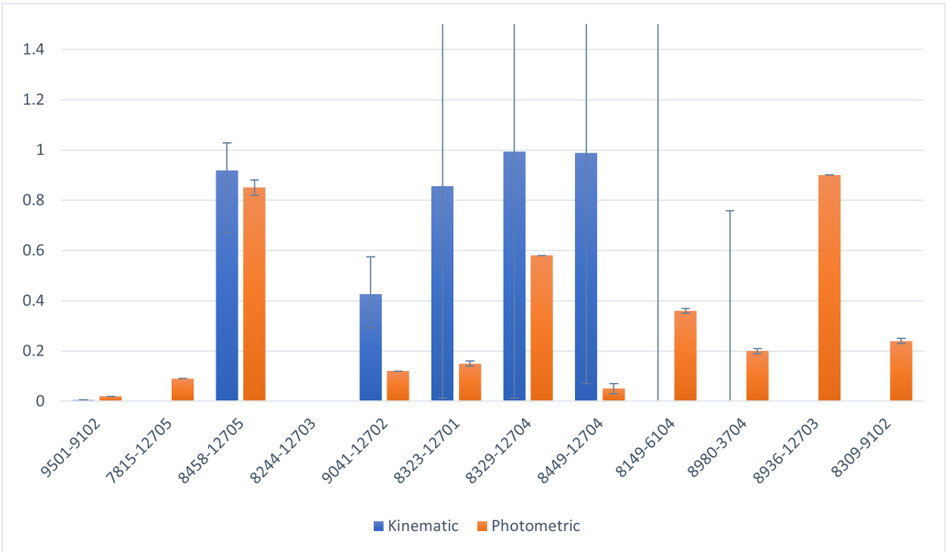

Figure 15: Photometric and Kinematic bulge mass fractions with error bars from table 4. For some galaxies the errors go off the graph. Clearly from the graph there is no similarity with the results from my kinematic data compared with the photometric data from Simard et al. (2011).

the DM fraction is on order of E-10/E-15 respectively. It is quite hard to compare since the order of error is extremely large and there is only one galaxy to compare. However using this method there is no agreement in DM fractions from kinematic and dynamical methods.

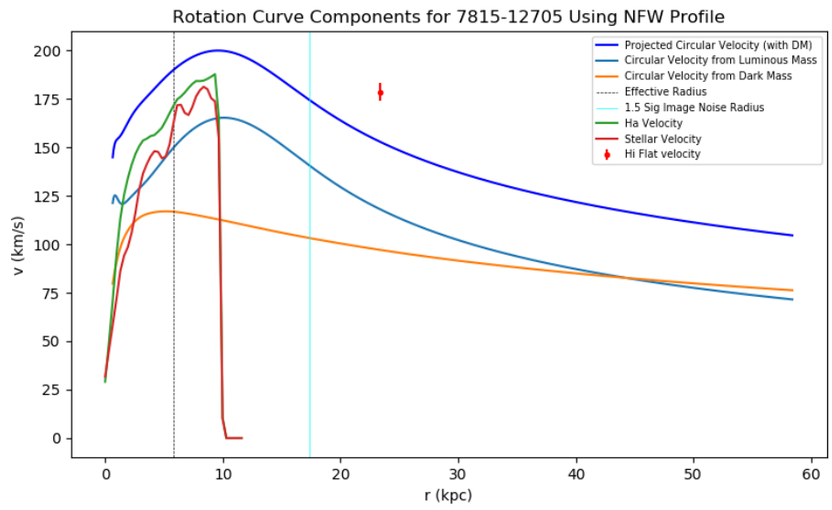

Figure 16: HI rotation curve for 7815-12705 (private communication, S. Campbell)

Overall the sample of galaxies used is too small and many have significant errors to be able to compare or get any useful conclusions from. The error limits for the mass fraction goes beyond 1 which is an impossibility. The method for obtaining the error will need improving. For many of the galaxies by eye there is small differences in the model fits with or without a dark halo. This is expected as the MaNGA survey only goes to 1.5Re of the galaxies radius.

Some errors in method include using mean values for the mass and scale heights for each galaxy however galaxies have varied mass and size and so this is not very accurate. When deriving a rotation curve beam smearing was ignored and this will give inaccuracies for the first few data points in the curve.

Asymmetric drift was not corrected for in any of the rotation curves. Due to gravitational interactions the orbit of the Hα gas is not perfectly circular, and the observed velocity will be lower than the velocity calculated (Weijmans et al., 2008).

I obtained Hα rotation curves and mass fractions for 12 disk galaxies with data from the MaNGA survey. Here are my results:

- By comparing the Hα and the HI rotation curves in the inner regions for galaxy 7815-12705 there is no agreement in dark matter mass decomposition.
- There is no correlation between the bulge/stellar mass and halo/total mass.
- There is no correlation between photometric and kinematic bulge fractions.

In future work obtaining a larger sample of galaxies to compare results to would give a more concrete conclusion.

References

Binney, J. and Tremaine, S. (2008). *Galactic Dynamics: Second Edition.*

Blanton, M. R., Kazin, E., Muna, D., Weaver, B. A., and Price-Whelan, A. (2011). Improved Background Subtraction for the Sloan Digital Sky Survey Images. , 142(1):31.

Bottema, R. and Pestaña, J. L. G. (2015). The distribution of dark and luminous matter inferred from extended rotation curves. , 448(3):2566–2593.

Bovy, J. (2015). galpy: A python Library for Galactic Dynamics. , 216(2):29.

Bundy, K., Bershady, M. A., Law, D. R., Yan, R., Drory, N., MacDonald, N., Wake, D. A., Cherinka, B., Sánchez-Gallego, J. R., Weijmans, A.-M., Thomas, D., Tremonti, C., Masters, K., Coccato, L., Diamond-Stanic, A. M., Aragón-Salamanca, A., Avila-Reese, V., Badenes, C., Falcón-Barroso, J., Belfiore, F., Bizyaev, D., Blanc, G. A., Bland-Hawthorn, J., Blanton, M. R., Brownstein, J. R., Byler, N., Cappellari, M., Conroy, C., Dutton, A. A., Emsellem, E., Etherington, J., Frinchaboy, P. M., Fu, H., Gunn, J. E., Harding, P.,

Johnston, E. J., Kauffmann, G., Kinemuchi, K., Klaene, M. A., Knapen, J. H., Leauthaud, A., Li, C., Lin, L., Maiolino, R., Malanushenko, V., Malanushenko, E., Mao, S., Maraston, C., McDermid, R. M., Merrifield, M. R., Nichol, R. C., Oravetz, D., Pan, K., Parejko, J. K., Sanchez, S. F., Schlegel, D., Simmons, A., Steele, O., Steinmetz, M., Thanjavur, K., Thompson, B. A., Tinker, J. L., van den Bosch, R. C. E., Westfall, K. B., Wilkinson, D., Wright, S., Xiao, T., and Zhang, K. (2015). Overview of the SDSS-IV MaNGA Survey: Mapping nearby Galaxies at Apache Point Observatory. , 798(1):7.

Cherinka, B., Andrews, B., Sanchez-Gallego, J., Brownstein, J., Argudo-Fernandez, M., Blanton, M., Bundy, K., Jones, A., Masters, K., Law, D. R., Rowlands, K., Weijmans, A., Westfall, K., and Yan, R. (2020). Marvin: A Toolkit for Streamlined Access and Visualisation of the SDSS-IV MaNGA Data Set. In Pizzo, R., Deul, E. R., Mol, J. D., de Plaa, J., and Verkouter, H., editors, *Astronomical Society of the Pacific Conference Series*, volume 527 of *Astronomical Society of the Pacific Conference Series*, page 743.

Freeman, K. C. (1970). On the Disks of Spiral and S0 Galaxies. , 160:811.

Granados, A., Torres, D., Castañeda, L., Henao-O., J., L., and Vanegas, S. (2017). GalRotpy: an educational tool to understand and parametrize the rotation curve and gravitational potential of disk-like galaxies. *arXiv e-prints*, page arXiv:1705.01665.

Kuzio de Naray, R., Arsenault, C. A., Spekkens, K., Sellwood, J. A., McDonald, M., Simon, J. D., and Teuben, P. (2012a). Searching for non-axisymmetries in NGC 6503: a weak end-on bar. , 427(3):2523–2536.

Kuzio de Naray, R., Arsenault, C. A., Spekkens, K., Sellwood, J. A., McDonald, M., Simon, J. D., and Teuben, P. (2012b). Searching for non-axisymmetries in NGC 6503: a weak end-on bar. , 427(3):2523–2536.

Masters, K. L., Stark, D. V., Pace, Z. J., Phipps, F., Rujopakarn, W., Samanso, N., Harrington, E., Sánchez-Gallego, J. R., Avila-Reese, V., Bershady, M., Cherinka, B., Fielder, C. E., Finnegan, D., Riffel, R. A., Rowlands, K., Shamsi, S., Newnham, L., Weijmans, A.-M., and Witherspoon, C. A. (2019). H I-MaNGA: H I follow-up for the MaNGA survey. , 488(3):3396–3405.

Navarro, J. F., Frenk, C. S., and White, S. D. M. (1996). The Structure of Cold Dark Matter Halos. , 462:563.

Planck Collaboration, Aghanim, N., Akrami, Y., Ashdown, M., Aumont, J., Baccigalupi, C., Ballardini, M., Banday, A. J., Barreiro, R. B., Bartolo, N., Basak, S., Battye, R., Benabed, K., Bernard, J. P., Bersanelli, M., Bielewicz, P., Bock, J. J., Bond, J. R., Borrill, J., Bouchet, F. R., Boulanger, F., Bucher, M., Burigana, C., Butler, R. C., Calabrese, E., Cardoso, J. F., Carron, J., Challinor, A., Chiang, H. C., Chluba, J., Colombo, L. P. L., Combet, C., Contreras, D., Crill, B. P., Cuttaia, F., de Bernardis, P., de Zotti, G., Delabrouille, J., Delouis, J. M., Di Valentino, E., Diego, J. M., Doré, O., Douspis, M., Ducout, A., Dupac, X., Dusini, S., Efstathiou, G., Elsner, F., Enßlin, T. A., Eriksen, H. K., Fantaye, Y., Farhang, M., Fergusson, J., Fernandez-Cobos, R., Finelli, F., Forastieri, F., Frailis, M., Fraisse, A. A., Franceschi, E., Frolov, A., Galeotta, S., Galli, S., Ganga, K., Génova-Santos, R. T., Gerbino, M., Ghosh, T., González-Nuevo, J., Górski, K. M., Gratton, S., Gruppuso, A., Gudmundsson, J. E., Hamann, J., Handley, W., Hansen, F. K., Herranz, D., Hildebrandt, S. R., Hivon, E., Huang, Z., Jaffe, A. H., Jones, W. C., Karakci, A., Keihänen, E., Keskitalo, R., Kiiveri, K., Kim, J., Kisner, T. S., Knox, L., Krachmalnicoff, N., Kunz, M., Kurki-Suonio, H., Lagache, G., Lamarre, J. M., Lasenby, A., Lattanzi, M., Lawrence, C. R., Le Jeune, M., Lemos, P., Lesgourgues, J., Levrier, F., Lewis, A., Liguori, M., Lilje, P. B., Lilley, M., Lindholm, V., López-Caniego, M., Lubin, P. M., Ma, Y. Z., Macías-Pérez, J. F., Maggio, G., Maino, D., Mandolesi, N., Mangilli, A., Marcos-Caballero, A., Maris, M., Martin, P. G., Martinelli, M., Martínez-González, E., Matarrese, S., Mauri, N., McEwen, J. D., Meinhold, P. R., Melchiorri, A., Mennella, A., Migliaccio, M., Millea, M., Mitra, S., Miville-Deschênes, M. A., Molinari, D., Montier, L., Morgante, G., Moss, A., Natoli, P., Nørgaard-Nielsen, H. U., Pagano, L., Paoletti, D., Partridge, B., Patanchon, G., Peiris, H. V., Perrotta, F., Pettorino, V., Piacentini, F., Polastri, L., Polenta, G., Puget, J. L., Rachen, J. P., Reinecke, M., Remazeilles, M.,

Renzi, A., Rocha, G., Rosset, C., Roudier, G., Rubiño-Martín, J. A., Ruiz-Granados, B., Salvati, L., Sandri, M., Savelainen, M., Scott, D., Shellard, E. P. S., Sirignano, C., Sirri, G., Spencer, L. D., Sunyaev, R., Suur-Uski, A. S., Tauber, J. A., Tavagnacco, D., Tenti, M., Toffolatti, L., Tomasi, M., Trombetti, T., Valenziano, L., Valiviita, J., Van Tent, B., Vibert, L., Vielva, P., Villa, F., Vittorio, N., Wandelt, B. D., Wehus, I. K., White, M., White, S. D. M., Zacchei, A., and Zonca, A. (2020). Planck 2018 results. VI. Cosmological parameters. , 641:A6.

Sellwood, J. A. and Spekkens, K. (2015). DiskFit: a code to fit simple non-axisymmetric galaxy models either to photometric images or to kinematic maps. *arXiv e-prints*, page arXiv:1509.07120.

Simard, L., Mendel, J. T., Patton, D. R., Ellison, S. L., and McConnachie, A. W. (2011). A Catalog of Bulge+disk Decompositions and Updated Photometry for 1.12 Million Galaxies in the Sloan Digital Sky Survey. , 196(1):11.

Sofue, Y. (2013). *Mass Distribution and Rotation Curve in the Galaxy*, volume 5, page 985.

Sofue, Y. (2016). Rotation curve decomposition for size-mass relations of bulge, disk, and dark halo components in spiral galaxies. , 68(1):2.

Sofue, Y. and Rubin, V. (2001). Rotation Curves of Spiral Galaxies. , 39:137–174.

Spekkens, K. and Sellwood, J. A. (2007). Modeling Noncircular Motions in Disk Galaxies: Application to NGC 2976. , 664(1):204–214.

Tiley, A. L., Swinbank, A. M., Harrison, C. M., Smail, I., Turner, O. J., Schaller, M., Stott, J. P., Sobral, D., Theuns, T., Sharples, R. M., Gillman, S., Bower, R. G., Bunker, A. J., Best, P., Richard, J., Bacon, R., Bureau, M., Cirasuolo, M., and Magdis, G. (2019). The shapes of the rotation curves of star-forming galaxies over the last ≈10 Gyr. , 485(1):934–960.

Weijmans, A.-M., Krajnović, D., van de Ven, G., Oosterloo, T. A., Morganti, R., and de Zeeuw, P. T. (2008). The shape of the dark matter halo in the early-type galaxy NGC 2974. , 383(4):1343–1358.